

## Accepted Manuscript

Determination of the Chiral Indices of Tungsten Disulfide (WS<sub>2</sub>) Nanotubes by Electron Diffraction

Hakan Deniz, Lu-Chang Qin

PII: S0009-2614(12)01100-1

DOI: <http://dx.doi.org/10.1016/j.cplett.2012.09.041>

Reference: CPLETT 30628

To appear in: *Chemical Physics Letters*

Received Date: 19 July 2012

Accepted Date: 20 September 2012



Please cite this article as: H. Deniz, L-C. Qin, Determination of the Chiral Indices of Tungsten Disulfide (WS<sub>2</sub>) Nanotubes by Electron Diffraction, *Chemical Physics Letters* (2012), doi: <http://dx.doi.org/10.1016/j.cplett.2012.09.041>

This is a PDF file of an unedited manuscript that has been accepted for publication. As a service to our customers we are providing this early version of the manuscript. The manuscript will undergo copyediting, typesetting, and review of the resulting proof before it is published in its final form. Please note that during the production process errors may be discovered which could affect the content, and all legal disclaimers that apply to the journal pertain.

1  
2  
3  
4 **Determination of the Chiral Indices of Tungsten Disulfide (WS<sub>2</sub>)**  
5  
6 **Nanotubes by Electron Diffraction**  
7  
8

9 Hakan Deniz\* and Lu-Chang Qin

10  
11 *Department of Physics and Astronomy, University of North Carolina at Chapel Hill,*  
12 *Chapel Hill, NC 27599-3255, USA*  
13  
14

15  
16 \* *Present address: Max-Planck Institute of Microstructure Physics*  
17 *Weinberg 2, 06120 Halle (Saale), Germany*  
18  
19  
20

21 **ABSTRACT**

22  
23 An electron diffraction method is described and applied to analyze the atomic  
24 structure of individual tungsten disulfide (WS<sub>2</sub>) nanotubes. The method is based on a  
25 recently developed zoning scheme to determine the chiral indices of nanotubes by nano-  
26 beam electron diffraction. The chiral indices of a WS<sub>2</sub> nanotube, which has its outermost  
27 shell missing on one end due to uneven growth of shells, is given to illustrate the  
28 indexing procedure. We also observed that the tubule chiralities within each WS<sub>2</sub>  
29 nanotube display a mono-helical structure on average with a dispersion of a few degrees.  
30  
31  
32  
33  
34  
35  
36

37 **INTRODUCTION**

38  
39 The successful synthesis of tungsten disulfide (WS<sub>2</sub>) nanotubes by Tenne *et al* in  
40 1992 proved that formation of tubular nanostructures is not unique to carbon.<sup>1</sup> This was  
41 followed by reports of other new types of nanotubes, such as MoS<sub>2</sub>, WSe<sub>2</sub>, MoSe<sub>2</sub>, BN,  
42 and GaN, in inorganic compounds with layered structures.<sup>2-5</sup> Other examples of metal  
43 disulfide nanotubes include TiS<sub>2</sub>, ZrS<sub>2</sub>, HfS<sub>2</sub>, VS<sub>2</sub>, NbS<sub>2</sub>, TaS<sub>2</sub> and ReS<sub>2</sub>.<sup>6-9</sup> The field of  
44 inorganic nanotube research has been growing steadily ever since. The atomic structure  
45 of a single shell of metal chalcogenides MX<sub>2</sub> (M=metal; X=S, Se, Te) can be described  
46 by a metal layer sandwiched between two chalcogen layers, forming a hexagonal cell.  
47 Triple layers are stacked like graphite with only van der Waals interactions between  
48 them. The WS<sub>2</sub> layers can be rolled into a cylindrical structure by choosing a specific  
49 direction in the two-dimensional (2D) crystal lattice. As for the case of carbon nanotubes  
50 (CNTs), this direction can be described by a chiral vector expressed by  $\vec{C} = u\vec{a}_1 + v\vec{a}_2$ ,  
51  
52  
53  
54  
55  
56  
57  
58  
59  
60  
61  
62  
63  
64  
65

1  
2  
3  
4 where  $\vec{a}_1$  and  $\vec{a}_2$  are the basis vectors of the crystal lattice with an inter-angle of  $60^\circ$  and  
5  
6  $u$  and  $v$  are two integers which are also named as chiral indices  $(u, v)$ . The diameter  $d$  of a  
7  
8 single-shell  $\text{WS}_2$  nanotube is given as  $d = a\sqrt{u^2 + v^2 + uv} / \pi$ , where  $a = 0.315$  nm is the  
9  
10 in-plane lattice constant of  $\text{WS}_2$ .<sup>10</sup>

11  
12  $\text{WS}_2$  nanotubes exhibit different characteristics from CNTs in terms of their  
13  
14 electronic properties. CNTs can be either metallic or semi-conducting depending on their  
15  
16 chiral indices, whereas  $\text{WS}_2$  ( $\text{MoS}_2$ ) nanotubes are predicted to be semi-conducting  
17  
18 regardless of their chirality.<sup>11-12</sup> Recently, this was confirmed by a scanning tunneling  
19  
20 microscopy study of  $\text{WS}_2$  nanotubes.<sup>13</sup> Synthesis, structure and self-assembly of sub-  
21  
22 nanometer single-shell  $\text{MoS}_2$  nanotubes of (3,3) armchair structure have been reported  
23  
24 recently with predictions that these tubules might be metallic with a small but finite  
25  
26 density of states at the Fermi level.<sup>14</sup> Although bulk  $\text{WS}_2$  ( $\text{MoS}_2$ ) nanotubes of armchair  
27  
28 structure have a small indirect and moderate direct band gap, it was calculated that zigzag  
29  
30  $\text{WS}_2$  ( $\text{MoS}_2$ ) nanotubes will have a small direct band gap whose energy is monotonically  
31  
32 increasing as a function of the diameter.<sup>11-12</sup> The report of the synthesis of single- or  
33  
34 multi-shell  $\text{WS}_2$  nanotubes on template multi-walled carbon nanotubes opens up new  
35  
36 possibilities for nano-composite materials and applications, such as solid lubricants,  
37  
38 catalysts, scanning probe microscopy tips.<sup>15-19</sup> It is therefore of fundamental importance  
39  
40 to have a complete and unambiguous determination of the atomic structure of  $\text{WS}_2$   
41  
42 nanotubes in order to understand the structure-property relationships of this  
43  
44 nanostructured material.

45  
46 The structure and defects of  $\text{WS}_2$  nanotubes have been studied by high-resolution  
47  
48 transmission electron microscopy (HRTEM) and electron diffraction (ED) extensively.  
49  
50 Early studies revealed their morphologies where open tips with occasional uneven shells  
51  
52 and defective shells were common.<sup>20</sup> Non-chiral nanotubes were mostly armchair type.  
53  
54 Thin nanotubes with diameter up to 30 nm were cylindrical whereas thick nanotubes with  
55  
56 diameter up to 150 nm had polygonal cross-sections.<sup>21</sup> It was observed that nanotube caps  
57  
58 could take rectangular or spherical form depending upon wall thickness and tubule  
59  
60 morphology. Nanotubes of mono- and multi-helical structures were identified. Dark-field  
61  
62 diffraction contrast imaging showed that mono-helical nanotubes with a dispersion of a  
63  
64 few degrees have right-handed chirality.<sup>22</sup> Aberration-corrected HRTEM and Moiré  
65

1  
2  
3  
4 pattern-based techniques combined with structure modeling and image simulations were  
5 utilized to obtain the chiral indices of WS<sub>2</sub> nanotubes for better understanding of their  
6 growth mechanism.<sup>23</sup>  
7  
8

9  
10 In this paper, we present a systematic procedure to identify the atomic structure of  
11 a five-shell WS<sub>2</sub> nanotube accurately using electron diffraction and the recently  
12 developed zoning scheme. To the best of our knowledge, this is the first time that the  
13 chiral indices (*u,v*) of an inorganic metal disulfide nanotube were determined  
14 unambiguously using electron diffraction.  
15  
16  
17  
18  
19

## 20 21 **METHOD OF ANALYSIS**

22  
23 Electron diffraction patterns (EDP) obtained from WS<sub>2</sub> nanotubes resemble very  
24 much to those of CNTs in terms of their appearance. Both kinds of nanotubes exhibit  
25 layer lines in their diffraction patterns due to the axial periodicity of the tubular structure.  
26 Based on the helical diffraction method developed for the determination of the chiral  
27 indices of single-walled and multi-walled CNTs,<sup>24-32</sup> we have extended the analytical  
28 method to inorganic nanotubes. A major difference of WS<sub>2</sub> nanotubes compared to their  
29 carbon counterparts is that they are composed of diatomic molecules. Although the  
30 electron scattering intensities of the layer lines from the WS<sub>2</sub> nanotubes are different  
31 from the elemental CNTs, their diffraction geometry remains the same. Therefore the  
32 well-established nano-beam electron diffraction method can also be used to determine the  
33 chirality (chiral indices) of composite nanotubes with a high accuracy.  
34  
35  
36  
37  
38  
39  
40  
41  
42

43 An electron diffraction pattern of WS<sub>2</sub> nanotube, similar to that of a CNT,  
44 consists of two sets of hexagonal spots in reciprocal space such that one set is caused by  
45 the top shell and the other by the bottom shell of the nanotube, as schematically  
46 illustrated in Fig. 1. The finite radial dimension of the nanotube manifests itself as  
47 diffraction spots elongated normal to the tubule axis. The diffraction pattern of a multi-  
48 shell nanotube is composed of a superposition of the reflections from all shells within the  
49 nanotube. For a helical single-shell WS<sub>2</sub> nanotube, there will be two sets of hexagonal  
50 reflections appearing as three sets of principal layer lines with respect to the equatorial  
51 line in the diffraction pattern. An armchair WS<sub>2</sub> nanotube will exhibit layer one layer line  
52 which is associated with the ( $\bar{1}0$ ) reflection while two layer lines associated with (01)  
53  
54  
55  
56  
57  
58  
59  
60  
61  
62  
63  
64  
65

1  
2  
3  
4 and (11) reflections will be observed for a zigzag tubule in the EDP. The spots associated  
5 with (02) reflections, which is the manifestation of interference effects due to the stacking  
6 of the shells, can also be seen in the EDP for multi-shell nanotubes.  
7  
8

9  
10 When the helicity of each shell of a multi-shell nanotube is different, there will be  
11 twice as many hexagonal sets as the number of shells in the diffraction pattern or three  
12 times as many principal layer lines on each side of the equatorial line. The first-order  
13 reflections of a multi-helicity nanotube can be divided into three zones where each shell  
14 with its distinct helicity will have a principal layer line in each of the three zones.<sup>32</sup> These  
15 zones are called Z1, Z2 and Z3 zones in reference to the labels of the layer lines in the  
16 EDP. The orientation of hexagonal reflections dictates that a zigzag tubule will have a  
17 layer line (L1) farthest away from the equator in the Z1 zone and an armchair tubule will  
18 have one closest. These two boundaries determine the width of the area (Z1 zone) in  
19 which the layer line L1 falls into for all other helicities whose helical angle varies  
20 between 0° and 30°. Similarly, the boundaries of other two zones can be determined and  
21 the sets of the layer lines corresponding to all helicities can be matched in an orderly  
22 fashion.<sup>33</sup> The layer lines L1 and L2 are coincident and the L3 line is located on the  
23 equator for an armchair tubule whereas the layer lines L2 and L3 coincide with each  
24 other for a zigzag tubule. As the helicity varies from 0° to 30°, the L1 and L2 layer lines  
25 move closer to each other and the L3 line moves towards the equatorial line.  
26  
27  
28  
29  
30  
31  
32  
33  
34  
35  
36  
37  
38

39 To determine the chiral indices ( $u, v$ ) with a high accuracy, their ratio  $v/u$  can be  
40 calculated using the measured layer line spacings  $D_1$  and  $D_2$  from the EDP and it can be  
41 expressed as<sup>29</sup>  
42  
43

$$\frac{v}{u} = \frac{2D_2 - D_1}{2D_1 - D_2} \quad (1)$$

44  
45  
46  
47  
48 This equation is not affected by either the tilt of the nanotube with respect to the incident  
49 electron beam or the camera length at which the EDP was taken.<sup>29</sup> The number of shells  
50 and their diameter can also be measured from the acquired high-resolution transmission  
51 electron microscope (HRTEM) images. In our analysis, the layer line spacings were  
52 measured digitally with automated software, which distinguishes and identifies the layer  
53 lines from the EDP according to user's specifications, in order to further improve the  
54 accuracy. After assigning each layer line into its respective helical set using the zoning  
55  
56  
57  
58  
59  
60  
61  
62  
63  
64  
65

1  
2  
3  
4 scheme, the index ratio  $v/u$  and its uncertainty were also calculated. This was followed by  
5 finding all possible chiral indices satisfying the measured  $v/u$  ratio within the  
6 experimental errors and matching the measured diameter closely.  
7  
8  
9

## 10 11 **EXPERIMENTAL**

12  
13 Transmission electron microscopy and electron diffraction study of  $WS_2$   
14 nanotubes were carried out with JEM-2010F operated at accelerating voltage of 200 kV.  
15 The sample was suspended in ethanol by sonication and then transferred onto a lacey  
16 carbon coated grid. A nano-probe was generated with the use of the 10  $\mu\text{m}$  condenser  
17 aperture by exciting the first condenser lens to maximum to obtain a smallest virtual  
18 source. Nano-beam diffraction patterns were collected using the parallel beam  
19 illumination conditions and recorded on both photographic films and CCD camera at the  
20 camera length of 40-60 cm. The diffraction patterns taken on CCD camera were used to  
21 measure the intensities on the layer lines since it has much a better dynamical range.  
22  
23  
24  
25  
26  
27  
28  
29

## 30 31 **RESULTS AND DISCUSSION**

32  
33 Figure 2(a) shows a high-resolution TEM image of a five-shell  $WS_2$  nanotube.  
34 The outermost shell of this nanotube is not continuous and does not extend to the end of  
35 the tubule. Therefore, the nanotube has five shells in one segment and only four shells in  
36 the other segment. This is indicated in Fig. 2 (b) where the arrows indicate the positions  
37 where the outermost shell ended. Two separate diffraction patterns, taken from the five-  
38 shell and four-shell segments, of this nanotube were obtained on the CCD camera in  
39 identical operational settings of the microscope and they are shown in Fig. 3 (a) and (b),  
40 respectively. The diameter of each shell was measured several times from the high-  
41 resolution TEM image averaged along the axis of the tubule to reduce the errors due to  
42 inconsistencies of measurements. The shell diameters are 16.10 nm, 14.82 nm, 13.61 nm,  
43 12.39 nm, and 11.07 nm in descending order with an uncertainty of  $\pm 0.07$  nm due to the  
44 finite pixel size in the CCD recorded image.  
45  
46  
47  
48  
49  
50  
51  
52  
53  
54

55 For both electron diffraction patterns, there is only one layer line in the first zone.  
56 Five layer lines can be identified in the second and the third zones of the diffraction  
57 pattern from the five-shell segment and four layer lines from the four-shell segment. The  
58  
59  
60  
61  
62  
63  
64  
65

small separations of the layer lines suggest that this nanotube has a multi-helicity structure with close helicities. The layer lines in the first zone are not resolved from each other due to insufficient resolution of the microscope and that of the recording media. It should also be noted that the width of zone Z1 is also the smallest. Therefore, the layer line spacings  $D_2$  and  $D_3$  were utilized in determining the  $v/u$  ratios to minimize the uncertainty. In this case, equation (1) is rewritten as

$$\frac{v}{u} = \frac{D_2 - D_3}{D_2 + 2D_3} \quad (2)$$

The error in the measurement of layer line spacing  $\sigma_D$  is used in estimating the error in the  $v/u$  ratio through  $\sigma_{v/u} = 3\sigma_D \sqrt{D_2^2 + 2D_3^2} / (D_2 + 2D_3)^2$  by error propagation of Equation (2).

Tables 1 and 2 show the measured layer line spacings from each diffraction pattern in arbitrary units and the grouping of the layer lines into their respective helical sets, which was done using the zoning scheme described in the previous section. The tables also list the ratio of the chiral indices  $v/u$  for each helicity present. The missing helicity (Group E) from Table 2 is due to the vanishing outermost shell. The layer lines in the second and third zones from both diffraction patterns indicate that groups C, D and E (ranking from lower to higher) should have the highest intensities and group A has the lowest among all (insets in Fig. 3 (a) and (b)). Figure 4 shows a comparison of the intensities of the first peak from the oscillations in the layer lines for each shell. Since the electron scattering amplitude in reciprocal space is proportional to the diameter of nanotube, this means that group E should have the largest diameter and group A the smallest among all shells. This suggests that the best assignment for group A is (101,21) and for group E is (151,21) using the measured diameters and the  $v/u$  ratios. This also means that the chiral indices of group B, group C, and group D should be (113,21), (126,21) and (139,21), respectively. Table 3 lists the final assignment of chiral indices for this five-shell WS<sub>2</sub> nanotube together with the diameter and helicity of each shell calculated from the assigned chiral indices. A comparison of the measured and calculated  $v/u$  ratios with their percent errors is also given in the table.

To improve further the accuracy of the index assignment, we also compared the electron intensity of the equatorial line obtained from the electron diffraction pattern of this nanotube with a simulated intensity calculated using the diameters deduced from the assigned chiral indices as shown in Fig. 5. The intensity of the equatorial layer line was calculated using the following equation:

$$I(R) = |F(R, L=0)|^2 = \left| f \sum_i^N d_i J_0(\pi R d_i) \right|^2, \quad (3)$$

where  $R$  is the radial distance from the axis in reciprocal space,  $f$  is the electron scattering factor,  $d_i$  is the diameter of the  $i$ -th shell,  $J_0$  is the Bessel function of order zero, and  $N$  is the total number of shells. Since  $\text{WS}_2$  is a binary compound, we used an average electron scattering factor defined by  $f = f_w + 2f_s$  in the simulations. As shown in Fig. 5, the assigned chiral indices give rise to a very good agreement of the diffraction peaks.

The nanotubes whose chiral indices have been determined in our study manifest a case that the helicity of each shell is only a few degrees apart from one another within a single nanotube. This suggests that the individual shells in the multi-shell  $\text{WS}_2$  nanotubes are strongly correlated. The nanotubes that we characterized also tend to have smaller chiral angles toward a zigzag structure (less than  $10^\circ$ ). No armchair or zigzag nanotube shells were ever observed in this study (see also Table 4). These observations are in agreement with previous findings,<sup>34</sup> but in contrary to the observations of a recent report that a single chiral shell embedded inside non-chiral shells behaves as a template in most cases for the growth of subsequent non-chiral shells within an individual multi-wall  $\text{WS}_2$  nanotube.<sup>23</sup>

The nanotubes studied in our work were synthesized in reduction and sulfidization of  $\text{WO}_3$  particles with  $\text{H}_2/\text{H}_2\text{S}$  gases in a fluidized-bed reactor.<sup>35</sup> Main characteristics of these nanotubes are large hollow cores, open-ended tips and small number of shells on average. This kind of growth mechanism produces mostly helical nanotubes and it was suggested that the helical growth were more favorable both energetically and kinetically because it could help to keep the growth front continuous at the tip of the nanotube. This is consistent with our observations of the zigzag-like



1  
2  
3  
4 orientation in these nanotubes. For this open-ended growth, we suggest that small  
5 variations in the growth rate at the tip were most likely the cause of observed small  
6 variations in the helicities. Since all shells are growing at the same time, the only way to  
7 compensate the changes in growth rate might be a slight change of the helicity in order to  
8 provide an even growth of all shells.  
9

10  
11  
12  
13 The example studied here showed monotonically changing helicities within a  
14 nanotube itself where a linear relationship can be drawn between the helicity and  
15 diameter whereas no such clear relation was seen for other tubules. This case may  
16 suggest that the structure of the nanotube will take the form of achiral type as the  
17 diameter increases. Based on this particular nanotube, we estimated that a tubule  
18 consisting of 13-14 shells would have an outermost shell with a diameter of about 28 nm  
19 with a zigzag structure and exhibit properties completely different than the bulk material.  
20 In this way, it might be possible to engineer the nanotube structure precisely for specific  
21 applications by controlling synthesis and growth conditions.  
22  
23  
24  
25  
26  
27  
28  
29

30 The average inter-shell spacing is 0.621 nm, which is only 0.2% larger than the  
31 known spacing of WS<sub>2</sub> but it ranged from the smallest of 0.594 nm to the largest of  
32 0.647 nm. A recent study showed that WS<sub>2</sub> is more compressible along the *c*-direction  
33 than the *a*-direction.<sup>36</sup> It was also observed the nanoparticle curvature modifies the local  
34 charging environment in the intra-shell and inter-shell directions compared to the bulk  
35 phase.<sup>37</sup> Such a large variation in inter-shell spacing might be explained by the  
36 cumulative effects of the nanotube curvature, sub-oxide contaminants between the shells,  
37 compression of the *c*-axis, and occasional structural defects as seen in the HRTEM image  
38 given in Fig. 2.  
39  
40  
41  
42  
43  
44  
45

46 Although the shells of the WS<sub>2</sub> nanotube in our study have such large diameters,  
47 the layer lines in the EDP, especially in the second and third zones, can still be  
48 distinguished from one another. The most serious limitation in determining the *v/u* ratios  
49 stems from the overlapping of the first layer line L1 of all shells within the nanotube due  
50 to small dispersion of the helicity. The overlapping layer lines can be problematic in  
51 general for any two shells with very close helical angles but this error is amplified for the  
52 first zone since it has the smallest width. Nonetheless, the electron diffraction method  
53 described in this paper can easily be adapted to determine the chiral indices of other  
54  
55  
56  
57  
58  
59  
60  
61  
62  
63  
64  
65

1  
2  
3  
4 inorganic nanotubes, such as BN and GaN and others cited in the introduction, formed  
5  
6 from the layered structures having a hexagonal crystal lattice.  
7  
8

## 9 10 CONCLUSIONS

11 The chiral indices of each and every shell of a five-shell WS<sub>2</sub> nanotube have been  
12 determined using electron diffraction. The helicities of the shells of this nanotube are  
13 different but are close to each other within less than 10°. This distribution of helicity is  
14 explained in terms of growth and formation of the nanotube. The experimental technique  
15 and method of analysis are generally applicable to all nanotubes with a cylindrical  
16 structure.  
17  
18  
19  
20  
21  
22  
23

## 24 ACKNOWLEDGEMENT

25 The authors wish to thank Professor R. Tenne for providing the tungsten disulfide  
26 nanotube samples used in this study.  
27  
28  
29  
30  
31

## 32 REFERENCES

- 33 (1) Tenne, R.; Margulis, L.; Genut, M.; Hodes, G. *Nature* **1992**, *360*, 444.  
34 (2) Feldman, Y.; Wasserman, E.; Srolovitz, D. J.; Tenne, R. *Science* **1995**, *267*, 222.  
35 (3) Nath, M.; Rao, C. N. R. *Chem. Comm.* **2001**, *21*, 2236.  
36 (4) Chopra, N. G.; Luyken, R. J.; Cherrey, K.; Crespi, V. H.; Cohen, M. L.; Louie, S.  
37 G.; Zettl, A. Boron nitride nanotubes. *Science* **1995**, *269*, 966.  
38 (5) Li, J. Y.; Chen, X. L.; Qiao, Z. Y.; Cao, Y. G.; Li, H. *J. Mater. Sci. Lett.* **2001**, *20*,  
39 1987.  
40 (6) Nath, M.; Rao, C. N. R. *Angew. Chem. Int. Ed.* **2002**, *41*, 3451.  
41 (7) Therese, H. A.; Rocker, F.; Reiber, A.; Li, J.; Stepputat, M.; Glasser, G.; Kolb, U.;  
42 Tremel, W. *Angew. Chem. Int. Ed.* **2005**, *44*, 262.  
43 (8) Nath, M.; Rao, C. N. R. *J. Am. Chem. Soc.* **2001**, *123*, 4841.  
44 (9) Brorson, M.; Hansen, T. W.; Jacobsen, C. J. H. *J. Am. Chem. Soc.* **2002**, *124*,  
45 11582.  
46 (10) Schutte, W. J.; de Boer, J. L.; Jellinek, F. *J. Solid State Chem.* **1987**, *70*, 207.  
47  
48  
49  
50  
51  
52  
53  
54  
55  
56  
57  
58  
59  
60  
61  
62  
63  
64  
65

- 1  
2  
3  
4 (11) Seifert, G.; Terrones, H.; Terrones, M.; Jungnickel, G.; Frauenheim, T. *Solid State*  
5 *Comm.* **2000**, *114*, 245.  
6  
7 (12) Seifert, G.; Terrones, H.; Terrones, M.; Jungnickel, G.; Frauenheim, T. *Phys. Rev.*  
8 *Lett.* **2000**, *85*, 146.  
9  
10 (13) Scheffer, L.; Rosentsveig, R.; Margolin, A.; Popovitz-Biro, R.; Seifert, G.; Cohen,  
11 S. R.; Tenne, R. *Phys. Chem. Chem. Phys.* **2002**, *4*, 2095.  
12  
13 (14) Remskar, M.; Mrzel, A.; Skraba, Z.; Jesih, A.; Ceh, M.; Demsar, J.; Stadelmann,  
14 P.; Levy, F.; Mihailovic, D. *Science* **2001**, *292*, 479.  
15  
16 (15) Whitby, R. L. D.; Hsu, W. K.; Fearon, P. K.; Billingham, N. C.; Maurin, I.; Kroto,  
17 H. W.; Walton, D. R. M.; Boothroyd, C. B.; Firth, S.; Clark, R. J. H.; Collison, D.  
18 *Chem. Mat.* **2002**, *14*, 2209.  
19  
20 (16) Whitby, R. L. D.; Hsu, W. K.; Boothroyd, C. B.; Kroto, H. W.; Walton, D. R. M.  
21 *Chem. Phys. Lett.* **2002**, *359*, 121.  
22  
23 (17) Rapoport, L.; Bilik, Y.; Feldman, Y.; Homyonfer, M.; Cohen, S. R.; Tenne, R.  
24 *Nature* **1997**, *387*, 791.  
25  
26 (18) Chen, J.; Li, S. L.; Xu, Q.; Tanaka, K. *Chem. Comm.* **2002**, *16*, 1722.  
27  
28 (19) Rothschild, A.; Cohen, S. R.; Tenne, R. *Appl. Phys. Lett.* **1999**, *75*, 4025.  
29  
30 (20) Rothschild, A.; Popovitz-Biro, R.; Lourie, O.; Tenne, R. *J. Phys. Chem. B* **2000**,  
31 *104*, 8976.  
32  
33 (21) Zhu, Y. Q.; Hsu, W. K.; Terrones, H.; Grobert, N.; Chang, B. H.; Terrones, M.;  
34 Wei, B. Q.; Kroto, H. W.; Walton, D. R. M.; Boothroyd, C. B.; Kinloch, I.; Chen,  
35 G. Z.; Windle, A. H.; Fray, D. J. *J. Mater. Chem.* **2000**, *10*, 2570.  
36  
37 (22) Margulis, L.; Dluzewski, P.; Feldman, Y.; Tenne, R. *J. Microsc.* **1996**, *181*, 68.  
38  
39 (23) Sadan, M. B.; Houben, L.; Enyashin, A. N.; Seifert, G.; Tenne, R. *Proc. Nat. Acad.*  
40 *Sci.* **2008**, *105*, 15643.  
41  
42 (24) Qin, L.-C. *J. Mater. Res.* **1994**, *9*, 2450.  
43  
44 (25) Lucas, A. A.; Bruynincks, V.; Lambin, Ph. *Europhys. Lett.* **1996**, *35*, 355.  
45  
46 (26) Qin, L.-C. Ichihashi, T.; Iijima, S. *Ultramicroscopy* **1997**, *67*, 181.  
47  
48 (27) Qin, L.-C. *Chem. Phys. Lett.* **1998**, *297*, 23.  
49  
50 (28) Gao, M.; Zuo, J. M.; Twesten, R. D.; Petrov, I.; Nagahara, L. A.; Zhang, R. *Appl.*  
51 *Phys. Lett.* **2003**, *82*, 2703.  
52  
53  
54  
55  
56  
57  
58  
59  
60  
61  
62  
63  
64  
65

- 1  
2  
3  
4 (29) Liu, Z.; Zhang, Q.; Qin, L.-C. *Appl. Phys. Lett.* **2006**, *86*, 191903.  
5  
6 (30) Qin, L.-C. *Rep. Prog. Phys.* **2006**, *69*, 2761.  
7  
8 (31) Qin, L.-C. *Phys. Chem. Chem. Phys.* **2007**, *9*, 31.  
9  
10 (32) Deniz, H.; Derbakova, A.; Qin, L.-C. *Ultramicroscopy* **2010**, *111*, 66.  
11  
12 (33) Deniz, H. *Ph.D. Thesis*, University of North Carolina at Chapel Hill, 2007.  
13  
14 (34) Rosentsveig, R.; Margolin, A.; Feldman, Y.; Popovitz-Biro, R.; Tenne, R. *Appl.*  
15 *Phys. A* **2002**, *74*, 367.  
16  
17 (35) Margolin, A.; Rosentsveig, R.; Albu-Yaron, A.; Popovitz-Biro, R.; Tenne, R. *J.*  
18 *Mater. Chem.* **2004**, *14*, 617.  
19  
20 (36) Selvi, E.; Yanzhang, M.; Aksoy, R.; Ertas, A.; White, A. *J. Phys. Chem. Sol.* **2006**,  
21 *67*, 2183.  
22  
23 (37) Luttrell, R. D.; Brown, S.; Cao, J.; Musfeldt, J. L.; Rosentsveig, R.; Tenne, R. *Phys.*  
24 *Rev. B* **2006**, *73*, 035410.  
25  
26  
27  
28  
29  
30  
31  
32  
33  
34  
35  
36  
37  
38  
39  
40  
41  
42  
43  
44  
45  
46  
47  
48  
49  
50  
51  
52  
53  
54  
55  
56  
57  
58  
59  
60  
61  
62  
63  
64  
65

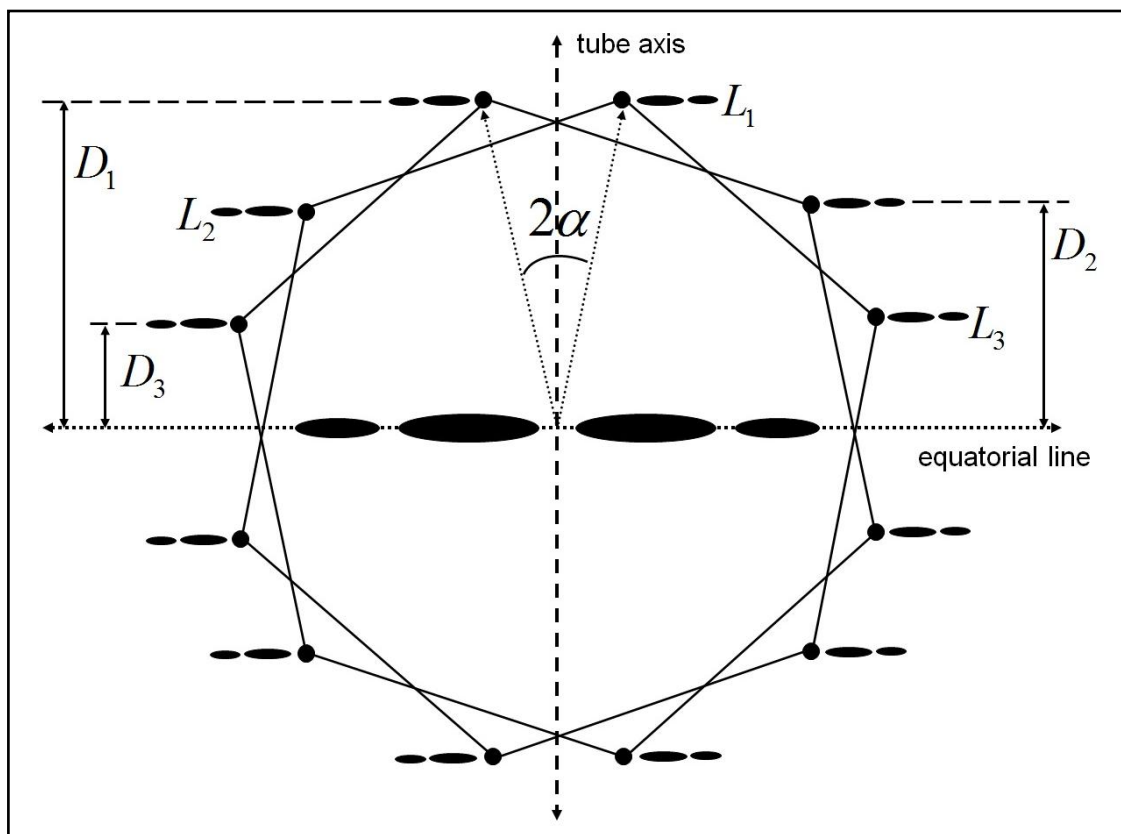


Figure 1. Schematic of electron diffraction pattern of a nanotube formed by a layered structure having a hexagonal lattice.  $\alpha$  is the helical angle or helicity of the tubule,  $L_1$ ,  $L_2$ , and  $L_3$  are the principal layer lines and  $D_1$ ,  $D_2$  and  $D_3$  are the layer line spacings in reciprocal space which are used for calculating the ratio of chiral indices  $v/u$ .

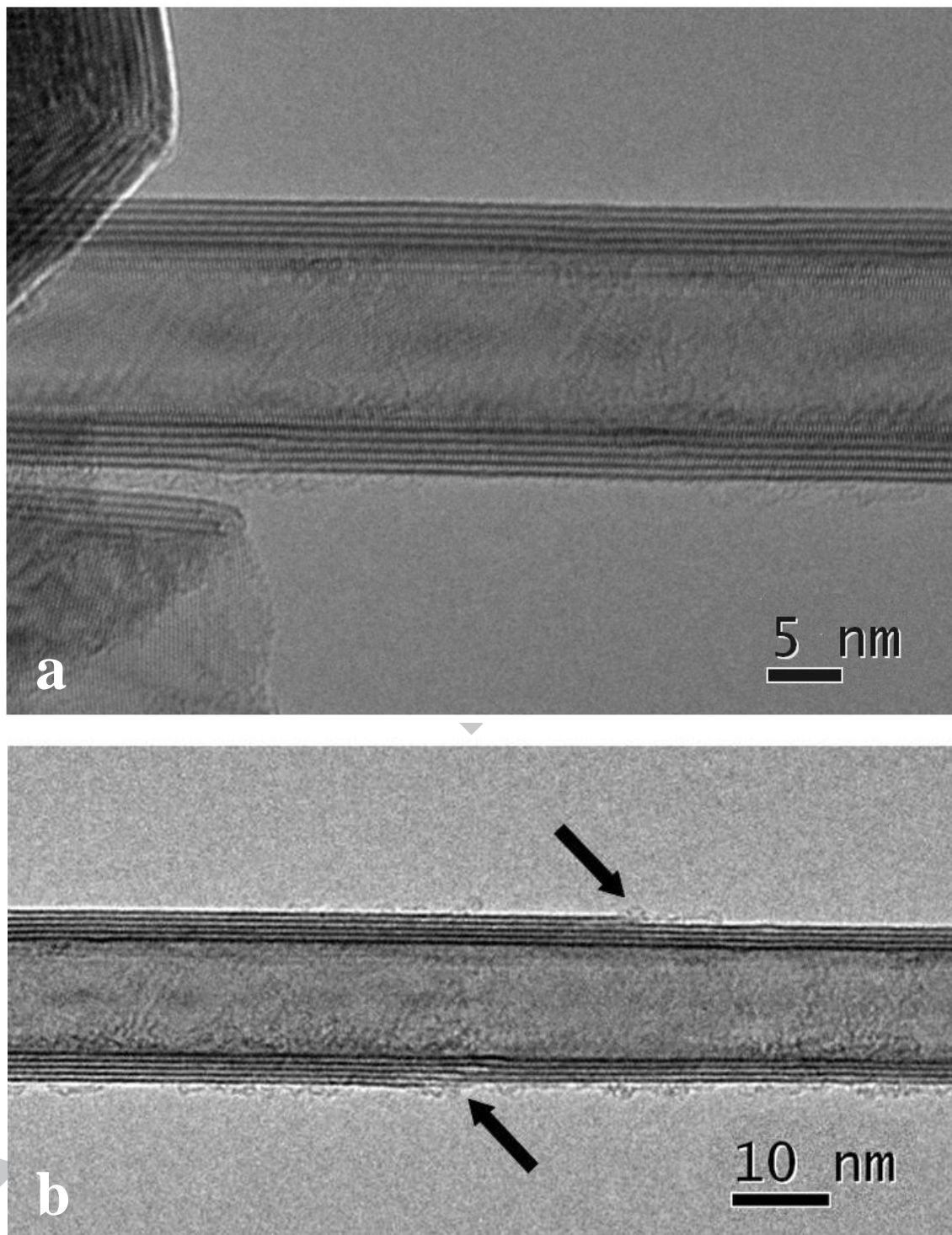
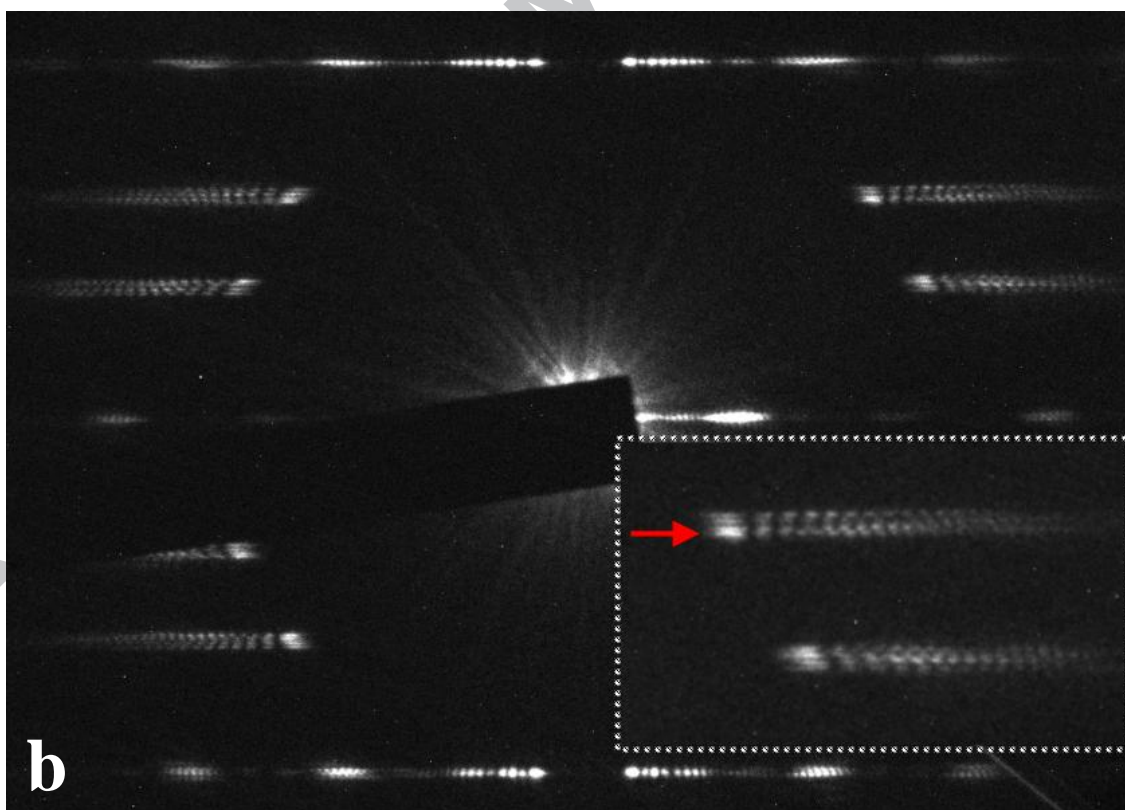
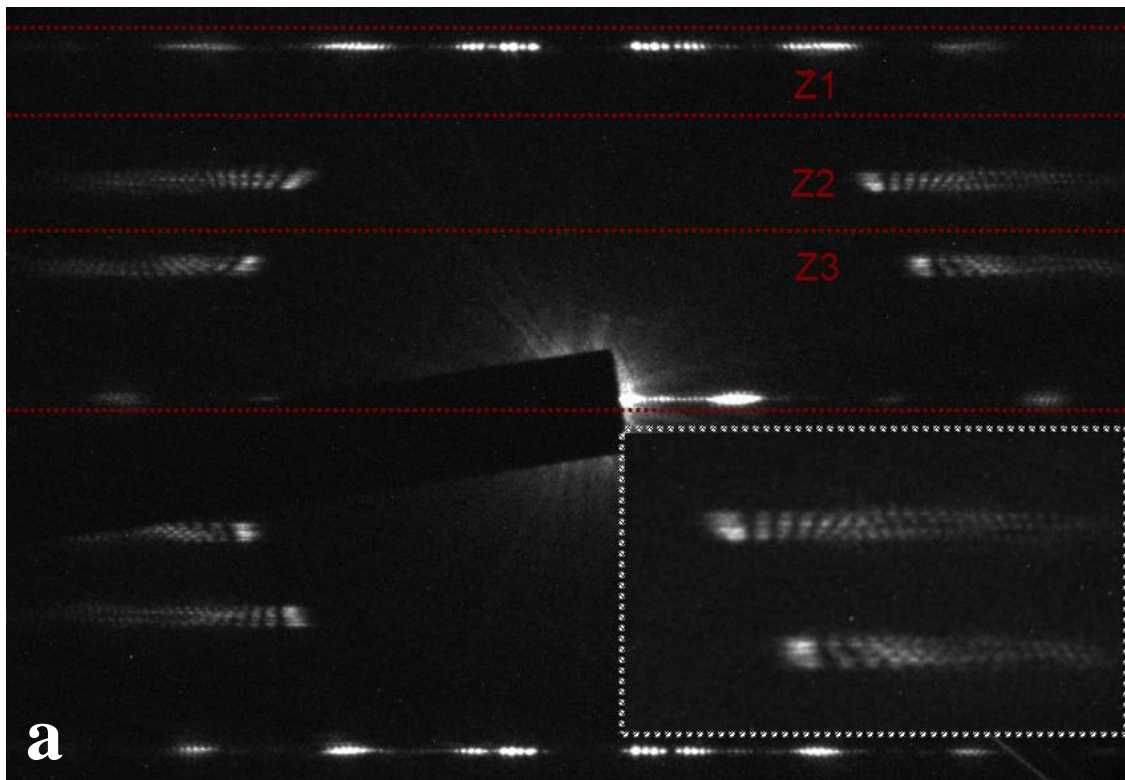


Figure 2. (a) High-resolution TEM image of a five-shell WS<sub>2</sub> nanotube near a fullerene-like WS<sub>2</sub> nanoparticle. (b) High-resolution TEM image of the same nanotube where the outermost layer of the nanotube vanished at locations indicated by arrows.

1  
2  
3  
4  
5  
6  
7  
8  
9  
10  
11  
12  
13  
14  
15  
16  
17  
18  
19  
20  
21  
22  
23  
24  
25  
26  
27  
28  
29  
30  
31  
32  
33  
34  
35  
36  
37  
38  
39  
40  
41  
42  
43  
44  
45  
46  
47  
48  
49  
50  
51  
52  
53  
54  
55  
56  
57  
58  
59  
60  
61  
62  
63  
64  
65



1  
2  
3  
4 Figure 3. (a) Electron diffraction pattern of the WS<sub>2</sub> nanotube acquired from the five-  
5 shell segment of the tubule on CCD camera. Three zones labeled Z1, Z2 and Z3,  
6 respectively, are indicated by the dotted red lines in the figure. The inset shows a  
7 magnified view of the layer lines where the five layer lines can be distinguished clearly in  
8 the Z2 and Z3 zones. (b) Electron diffraction pattern of the same tubule obtained from the  
9 part of the tubule with four shells. Again, the inset shows a magnified view of the layer  
10 lines (with four lines in Z2 and Z3 zones) where the red arrow points to the layer lines  
11 with higher intensity.  
12  
13  
14  
15  
16  
17  
18  
19  
20  
21  
22  
23  
24  
25  
26  
27  
28  
29  
30  
31  
32  
33  
34  
35  
36  
37  
38  
39  
40  
41  
42  
43  
44  
45  
46  
47  
48  
49  
50  
51  
52  
53  
54  
55  
56  
57  
58  
59  
60  
61  
62  
63  
64  
65



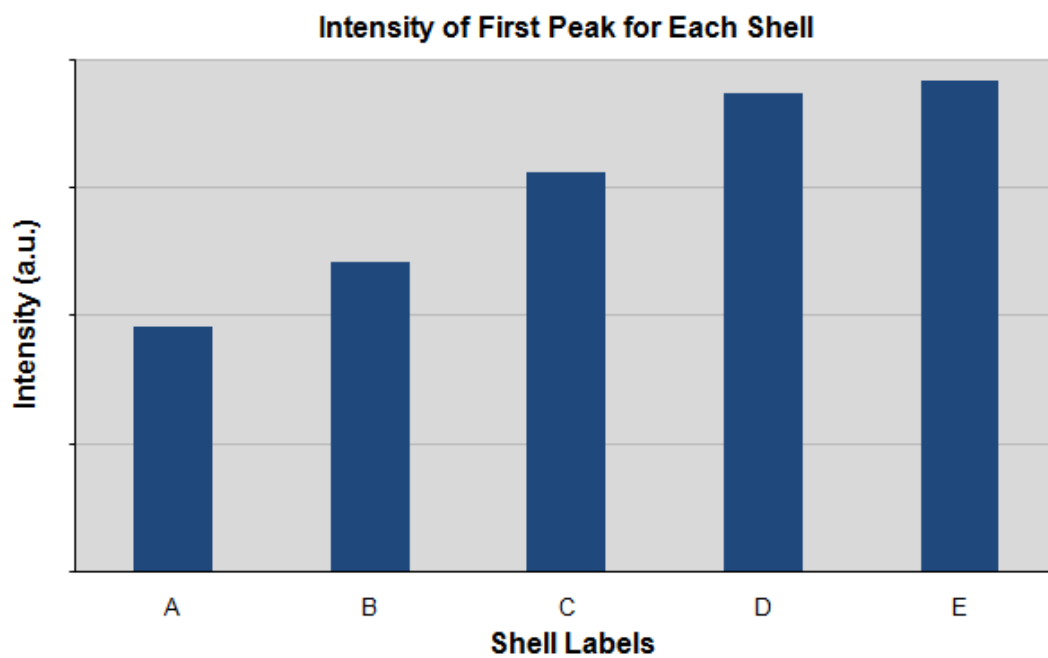


Figure 4. Plot shows the integrated intensity of the first peak obtained from the oscillations in the layer lines L2 of the diffraction pattern shown in Fig. 3a for each shell in the WS<sub>2</sub> nanotube.

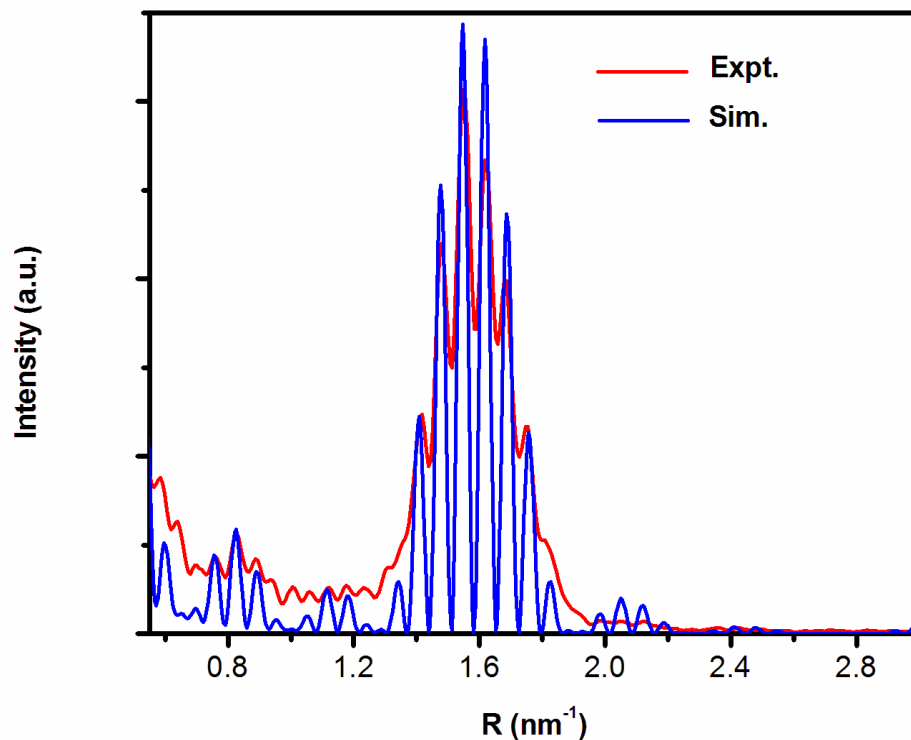


Figure 5. Comparison of experimental intensity (red) of the equatorial layer line and the simulated intensity (blue) using the deduced chiral indices. The intensity profile are given up to  $3 \text{ nm}^{-1}$  in the reciprocal space to include the (02) reflection. Fine modulations in the simulated curve are in good agreement with the experimental intensity.

Table 1. Experimentally measured layer line spacings (in arbitrary unit)  $D_1$ ,  $D_2$  and  $D_3$ , uncertainty in layer line spacing  $\sigma_D$ , index ratio  $v/u$ , and their propagated errors as percentage for the five-shell WS<sub>2</sub> nanotube shown in Fig. 2.

Group	$D_1$	$D_2$	$D_3$	$\sigma_D$	$v/u$	$\sigma_{v/u}$
A	530.9	339.2	189.1	2.6	0.209	2.8
B		335.8	196.0	1.0	0.192	1.1
C		327.5	202.0	1.4	0.172	1.8
D		323.5	208.4	1.0	0.156	1.4
E		319.3	212.0	0.3	0.144	0.5

Table 2. Experimentally measured layer line spacings (in arbitrary unit)  $D_1$ ,  $D_2$  and  $D_3$ , uncertainty in layer line spacing  $\sigma_D$ , index ratio  $v/u$ , and their propagated errors as percentage for the four-shell segment of the WS<sub>2</sub> nanotube shown in Fig. 2.

Group	$D_1$	$D_2$	$D_3$	$\sigma_D$	$v/u$	$\sigma_{v/u}$
A	529.8	342.4	188.3	1.0	0.214	1.0
B		334.2	192.3	3.3	0.197	3.7
C		327.2	200.4	2.2	0.174	2.7
D		323.7	205.0	1.1	0.162	1.4

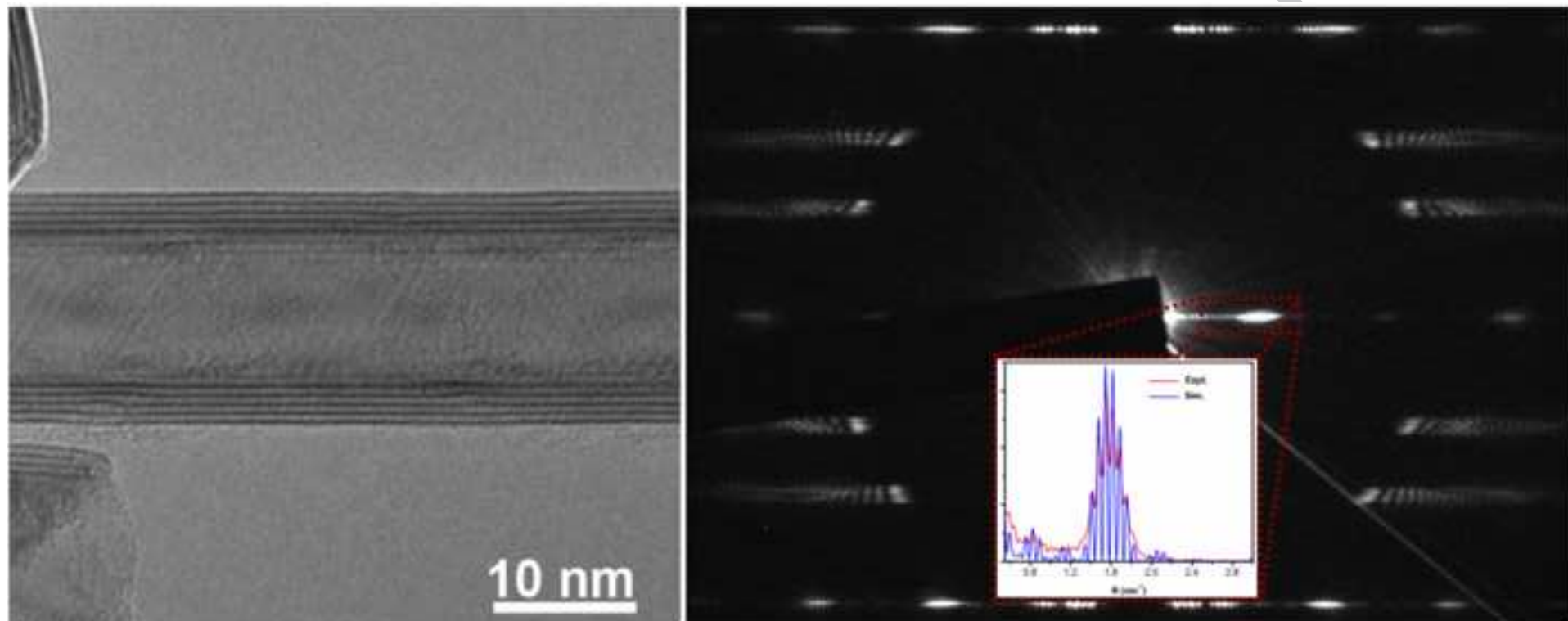
Table 3. Final assignment of chiral indices ( $u, v$ ) for the five-shell WS<sub>2</sub> nanotube with an incomplete outer shell together with the diameters and helicities calculated from the assigned indices. The percent error between the assigned and experimental  $v/u$  ratios is also listed.

Group	$u$	$v$	$d$ (nm)	$v/u$	$v/u$ -exp	%error	$\alpha$ (DEG)
A	101	21	11.33	0.208	0.209	-0.7	9.26
B	113	21	12.52	0.186	0.192	-3.2	8.38
C	126	21	13.81	0.167	0.172	-2.8	7.59
D	139	21	15.10	0.151	0.156	-2.9	6.94
E	151	21	16.30	0.139	0.144	-3.7	6.42

Table 4. Chiral indices ( $u,v$ ) of three additional WS<sub>2</sub> nanotubes analyzed.

WS <sub>2</sub> NT	Chiral Indices ( $u,v$ )				
	Shell 1	Shell 2	Shell 3	Shell 4	Shell 5
1	(97,23)	(108,25)	(116,31)	(132,25)	(141,29)
2	(80,19)	(95,15)	(102,22)	(113,22)	(125,22)
3	(90,39)	(98,47)	(112,46)		

ACCEPTED MANUSCRIPT



**Research Highlights**

- An electron diffraction method is described to obtain the chiral indices of nanotubes.
- The chiral indices of each shell of a compound WS<sub>2</sub> nanotube are determined.
- The WS<sub>2</sub> nanotube is nearly mono-helical with a small dispersion of helicity.

ACCEPTED MANUSCRIPT